

Adsorbed Polyelectrolyte Coatings Decrease Fe⁰ Nanoparticle Reactivity with TCE in Water: Conceptual Model and Mechanisms

TANAPON PHENRAT,^{†,‡} YUEQIANG LIU,[‡]
ROBERT D. TILTON,^{†,§,||} AND
GREGORY V. LOWRY^{*,†,‡,§}

Center for Environmental Implications of NanoTechnology (CEINT) and Departments of Civil & Environmental Engineering, Chemical Engineering, and Biomedical Engineering, Carnegie Mellon University, Pittsburgh, Pennsylvania 15213-3890

Received August 7, 2008. Revised manuscript received January 3, 2009. Accepted January 5, 2009.

The surfaces of reactive nanoscale zerovalent iron (NZVI) particles used for in situ groundwater remediation are modified with polymers or polyelectrolytes to enhance colloidal stability and mobility in the subsurface. However, surface modification decreases NZVI reactivity. Here, the TCE dechlorination rate and reaction products are measured as a function of adsorbed polyelectrolyte mass for three commercially available polyelectrolytes used for NZVI surface modification including poly(styrene sulfonate) (PSS), carboxymethyl cellulose (CMC), and polyaspartate (PAP). The adsorbed mass, extended layer thickness, and TCE-polyelectrolyte partition coefficient are measured and used to explain the effect of adsorbed polyelectrolyte on NZVI reactivity. For all modifiers, the dechlorination rate constant decreased nonlinearly with increasing surface excess, with a maximum of a 24-fold decrease in reactivity. The TCE dechlorination pathways were not affected. Consistent with Scheutjens–Fleer theory for homopolymer adsorption, the nonlinear relationship between the dechlorination rate and the surface excess of adsorbed polyelectrolyte suggests that adsorbed polyelectrolyte decreases reactivity primarily by blocking reactive surface sites at low surface excess where they adsorb relatively flat onto the NZVI surface, and by a combination of site blocking and decreasing the aqueous TCE concentration at the NZVI surface due to partitioning of TCE to adsorbed polyelectrolytes. This explanation is also consistent with the effect of adsorbed polyelectrolyte on acetylene formation. This conceptual model should apply to other medium and high molecular weight polymeric surface modifiers on nanoparticles, and potentially to adsorbed natural organic matter.

Introduction

The fate and reactivity of manufactured nanoparticles released into the environment is of great interest due to their

increasing use in consumer products and their potential risks to the environment and human health (1). Most nanomaterials are manufactured with an engineered surface coating to provide specific functionality (2–5), or will acquire a coating (e.g., natural organic matter) (6) once released into the environment which can affect their mobility and reactivity. Adsorbed coatings can affect particle surface reactivity by (1) inhibiting diffusion and adsorption of substrates to reactive surface sites, (2) decreasing the reaction rate at the surface by blocking access to reactive sites, or (3) inhibiting the desorption and diffusion of reaction products from the surface (7). Currently, a mechanistic understanding of how surface coatings affect the reactivity of manufactured nanoparticles in the environment is lacking.

Reactive nanoscale iron particles (RNIP) are one example of a manufactured reactive nanoparticle. These nanoscale zerovalent iron (NZVI) particles have been engineered with a surface coating such as poly(styrene sulfonate), polyaspartate, carboxymethyl cellulose, or triblock copolymers to inhibit aggregation (2, 3) and increase their mobility in the subsurface (8, 9). The reactivity of bare and surface-coated NZVI with a variety of environmental contaminants such as chlorinated organics (10–13), metals (14), and pesticides (15) has been extensively studied. During trichloroethylene (TCE) dechlorination by RNIP, TCE is reduced to nonhalogenated intermediates and byproducts including acetylene, ethylene, and ethane while zerovalent iron is oxidized (16, 17). The major reaction pathway is reductive β -elimination to form acetylene (10, 17) but hydrogenolysis (resulting in formation of chlorinated intermediates or products) and hydrogenation can also occur (17, 18). In a competing process, water (H⁺) can be reduced to H₂ (16). Adsorbed polyelectrolytes (9, 19) as well as adsorbed natural organic matter (20) have been shown to decrease the reactivity of NZVI or ZVI with target contaminants, but the mechanisms behind the decreased reactivity are not clear. Further, it is not known if adsorbed polyelectrolytes affect the reaction pathways and products formed from TCE degradation.

Reductive TCE dechlorination by NZVI is a surface-mediated reaction. For bare NZVI, mass transfer limitations from TCE diffusion through a stagnant water layer between the particle surface and bulk liquid is typically overcome by efficient mixing and ignored (4, 10, 12). This may not be the case for NZVI with an adsorbed polyelectrolyte layer. Based on the Scheutjens and Fleer conceptual model for homopolymer adsorption to the solid–water interface, charged homopolyelectrolytes are adsorbed onto the surface in a train–loop–tail orientation (Figure 1a). Trains are polymer sequences contacting the particle surface. Loops are stretches of polymer that do not touch the surface but connect two trains. Tails are polymer segments with only one end attached to the surface (21). Loops and tails form a stagnant polyelectrolyte layer between the NZVI surface and the bulk aqueous phase (Figure 1a) which could inhibit mass transfer or decrease the availability of contaminants to the NZVI surface due to partitioning to the hydrophobic backbone of the polyelectrolyte. The adsorbed layer thickness and the corresponding hydrodynamic resistance can be estimated from measurements of the electrophoretic mobility of polyelectrolyte-modified NZVI at ionic strengths ranging from 5 to 60 mM (NaCl) using Ohshima's soft particle theory (2, 22). Details of the application of this theory to polyelectrolyte-modified RNIP were recently reported (2). In addition to inhibiting mass transfer or decreasing the pollutant availability, adsorbed polyelectrolyte trains may directly block reactive sites of the NZVI surface. This could completely stop

* Corresponding author phone: 412-268-2948; fax: 412-268-7813; e-mail: glowry@cmu.edu.

[†] Center for Environmental Implications of NanoTechnology.

[‡] Civil & Environmental Engineering.

[§] Chemical Engineering.

^{||} Biomedical Engineering.

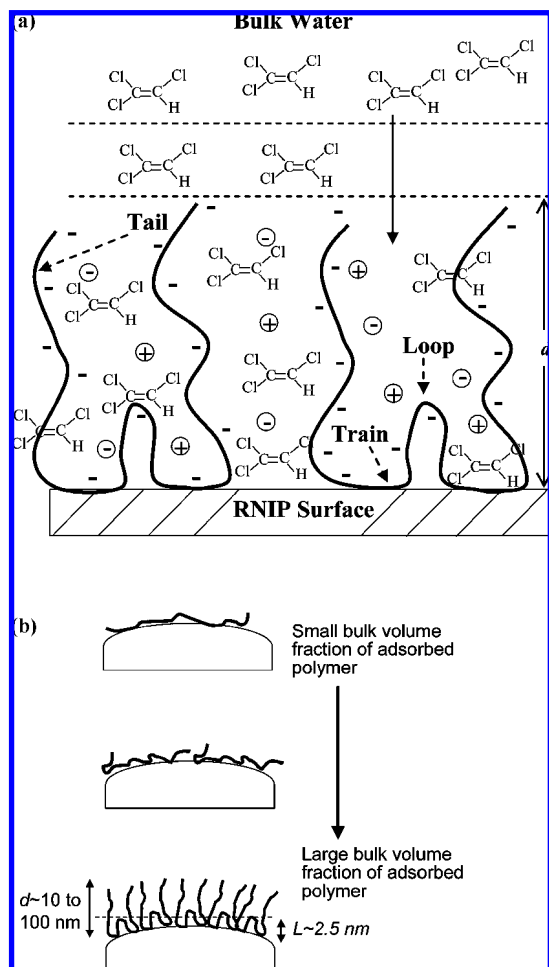


FIGURE 1. Schematic illustrating (a) site blocking due to adsorbed trains and tails, and (b) development of trains, loops and tails as a function of adsorbed polyelectrolyte mass according to the Scheutjens and Fler conceptual model for homopolymer adsorption (21).

or inhibit electron transfer from the NZVI surface to TCE depending on the separation distance between the NZVI surface and adsorbed TCE (23). Thus, adsorbed polyelectrolyte can potentially decrease NZVI reactivity with TCE due to blocking of reactive sites, mass transfer limitation due to inhibited TCE diffusion through the stagnant polyelectrolyte layer, or decreasing TCE availability at the particle surface.

A mechanistic understanding of how adsorbed polyelectrolytes affect the TCE dechlorination rate and the reaction products formed could enable the design of surface modifiers that enhance NZVI mobility with minimal impact on reactivity. The objective of this study is to determine the mechanisms by which adsorbed polyelectrolytes affect the TCE dechlorination rate by RNIP and the reaction products formed. Three commercially available polyelectrolytes, poly(styrene sulfonate) (PSS), carboxymethyl cellulose (CMC), and polyaspartate (PAP), are used as representative modifiers and because they provide different adsorbed layer properties (2). The TCE dechlorination rate and reaction products formed are measured for RNIP at different adsorbed mass of polyelectrolyte. The measured adsorbed polyelectrolyte layer properties (2), TCE degradation rates, and polymer–water partition coefficients are interpreted conceptually in the context of the Scheutjens and Fler self-consistent field model for homopolymer adsorption to gain insight about the relative

effects of site blocking, mass transfer resistance, and TCE availability on the observed rate of TCE dechlorination.

Materials and Methods

Chemicals. TCE (99.5+%) was from Aldrich. Sodium bicarbonate (99%) was from Fisher Scientific. Acetylene (1000 ppm and 1%), ethylene (1%), ethane (1%), vinyl chloride (VC) (10 ppm), and hydrogen (1.08%) standards were from Alltech. The balance of each gas standard was N_2 . Ultra high purity argon, hydrogen (5.18%), and N_2 were from Butler Gas products (Pittsburgh, PA).

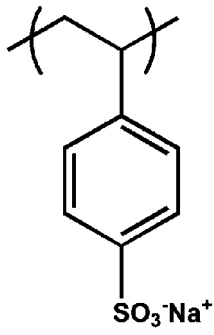
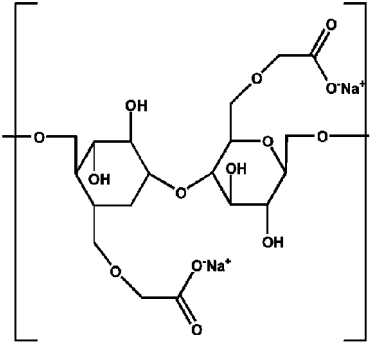
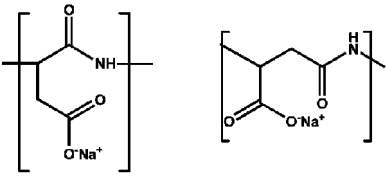
Fe^0/Fe_3O_4 Nanoparticles. Reactive nanoscale iron particles (RNIP), commercially available reactive Fe^0/Fe_3O_4 core–shell NZVI particles, were obtained from Toda Kogyo (Onada, Japan). The physical and chemical properties of RNIP have been previously reported (11, 17, 24). The Fe^0/Fe_3O_4 of bare RNIP used in this study was 26%/74% and its isoelectric point was $pH_{iep} = 6.3$. Prior to use, RNIP was stored as an aqueous slurry (pH 10.6) at approximately 300 g/L in an anaerobic chamber. From this slurry, a stock dispersion (10 mL at ~ 120 g/L) was prepared in 1 mM $NaHCO_3$ followed by ultrasonication for 30 min to break aggregates formed during storage. This sonicated stock dispersion was then diluted again with 1 mM $NaHCO_3$ to ~ 6 g/L. The N_2 –BET specific surface area of RNIP was ~ 15 m^2/g . The Fe^0 content of the particles was determined from acid digestion and monitoring hydrogen evolution as previously described (17). The detailed procedure is available in the Supporting Information.

Polyelectrolytes. PSS and CMC were from Aldrich (St. Louis, MO). PAP with a molecular weight of 2–3 kg/mol and 10 kg/mol was from Lanxess (Pittsburgh, PA) and NanoChem Solutions Inc. (Bedford Park, IL), respectively. Table 1 summarizes the properties and structure of each modifier. PSS and PAP stock solutions used to modify RNIP were prepared at 4 g/L in 1 mM $NaHCO_3$ and agitated using an orbital shaker at 25 °C for 12 h prior to physisorption to RNIP. CMC stock solutions were prepared similarly but agitated using an orbital shaker and refrigerated overnight to ensure complete hydration and dissolution.

Washed Polyelectrolyte-Modified RNIP Dispersions. RNIP dispersions with different adsorbed polyelectrolyte masses were prepared in 40 mL vials with anoxic solutions containing 3 g/L RNIP and between 0.005 and 1 g/L polyelectrolytes in 1 mM $NaHCO_3$. The pH of the mixtures ranged from 9.5 to 10.5 due to the oxidation of Fe^0 in the particles and subsequent production of OH^- (16). The isoelectric point of bare RNIP is $pH_{iep} = 6.3$. Therefore, both bare RNIP and polyelectrolytes are negatively charged in this study. Nevertheless, the specific interactions between the polyelectrolytes and the iron oxide surface are sufficiently strong to overcome the net electrostatic repulsion between the polyelectrolytes and the RNIP surface (2). After 48-h equilibration on a 30 rpm end-over-end rotator the dispersions were centrifuged at 27,500 rpm ($\sim 1.5 \times 10^{-5}g$) for 80 min, decanted, and refilled with 1 mM $NaHCO_3$ solution that had been purged with N_2 to remove oxygen. This process was repeated two more times to remove excess free polymer in solution prior to use in reactivity studies. The maximum irreversibly adsorbed polyelectrolyte surface excess concentration (Γ_{max}) and the adsorbed layer thickness (d) of each washed polyelectrolyte-modified RNIP are summarized in Table 2 as previously reported (2). Details of the solution-depletion method used to determine the adsorbed polyelectrolyte surface excess concentration (Γ), electrophoretic mobility, and Ohshima's soft particle analysis used to determine the adsorbed layer thickness (d) are in Phenrat et al. (2).

TCE Partitioning into Polyelectrolyte–Water Solutions. To qualitatively assess the partitioning of TCE between the

TABLE 1. Properties and Structure of Surface Modifiers.

Code	Chemical name /category	M_w^a (kg/mole)	D_p^b	K_p^c	Structure
PSS70K	Poly(styrene sulfonate) /anionic polyelectrolyte	70	340	11.5±2.4	
PSS1M		1,000	4,850	18.2±1.7	
CMC90K	Carboxymethylcellulose /anionic polysaccharide	90	342	11.9±2.4	
CMC700K		700	2,661	15.2±0.4	
PAP2.5K	Polyaspartate /anionic biopolymer	2-3	16	7.3±2.1	
PAP10K		10	64	7.9±1.5	

^a Molecular weight of the polyelectrolytes (g/mol), M_w , as specified by the manufacturers. ^b Average degree of polymerization, D_p , is estimated by dividing M_w of a polymer by the molecular weight of a monomer unit. ^c Reported error is one standard deviation from the mean of K_p (dimensionless) measured at polyelectrolyte concentrations of 5 and 10 g/L.

TABLE 2. Measured Fe^0 Content, Estimated Characteristics of Adsorbed Layer, and Calculated Half-life Time (τ) of TCE for Each Polyelectrolyte-Modified RNIP

code	Fe^0 content ^a (%)	Γ_{max} (mg/m ²)	d^b (nm)	$k_{TCE-obs}^c$ (10^{-3} L m ⁻² hr ⁻¹)	τ^d (day)
bare	26 ± 0.4	0	0	3.51 ± 0.42	0.4
PSS70K	15 ± 0.0	2.06 ± 0.27	67 ± 7	0.73 ± 0.03	1.9
PSS1M	15 ± 0.5	1.92 ± 0.24	198 ± 30	0.44 ± 0.04	3.2
CMC90K	24 ± 0.2	0.98 ± 0.16	7.2 ± 3.2	0.31 ± 0.02	4.5
CMC700K	29 ± 1.0	2.03 ± 0.08	40 ± 6.5	0.38 ± 0.03	3.7
PAP2.5K	24 ± 0.4	2.29 ± 0.23	40 ± 12	0.15 ± 0.01	9.3
PAP10K	25 ± 0.9	2.20 ± 0.35	44 ± 13	0.14 ± 0.01	9.9

^a Reported error is standard deviation of the mean of duplicates. ^b Based on Ohshima's soft particle analysis at the maximum surface excess (2). ^c Reported error is the standard deviation calculated from the upper and lower 95% confidence interval limits of k_{obs} measured in duplicate reactors. ^d Assumes 2 g/L of RNIP in porewater.

aqueous phase and an adsorbed polyelectrolyte layer, TCE partitioning between polymer and water was determined in 70 mL serum bottles capped by Teflon Mininert valves. Each reactor contained 40 mL of headspace and 30 mL of solution with either 5 or 10 g/L for each polyelectrolyte at pH 9, 0.04

mM TCE, and 1 mM $NaHCO_3$. A reactor without polyelectrolyte was prepared as a reference. The reactors were equilibrated on an end-over-end rotator at 30 rpm at 23 ± 2 °C for 12 h. After equilibration, the reactors were placed into a water bath at 25 °C for an hour prior to the headspace

measurement. A 100 μL headspace sample was withdrawn from the reactors and analyzed for TCE using a 30 m GSQ PLOT capillary column on a HP 6890 GC/FID as described in Liu et al. (17). Measurements were performed in duplicate. The difference in the equilibrium aqueous TCE concentration of the reference reactor and the reactor with each polyelectrolyte was attributed to partitioning of TCE into the polyelectrolyte/water mixture. The TCE polyelectrolyte/water partition coefficient (dimensionless), K_p ($\text{mol/L}_{\text{poly}}/\text{mol/L}_{\text{water}}$) is calculated using eq 1

$$\frac{C_{\text{TCE}}^{\text{poly}}}{C_{\text{TCE}}^{\text{water}}} = K_p = \frac{\left[(C_{\text{TCE}}^{\text{Air}} V_{\text{hs}})_{\text{ref}} - (C_{\text{TCE}}^{\text{Air}} V_{\text{hs}})_{\text{poly}} + \left(\frac{C_{\text{TCE}}^{\text{Air}} V_{\text{water}}}{K_{\text{H}}^{\text{TCE*}}} \right)_{\text{ref}} - \left(\frac{C_{\text{TCE}}^{\text{Air}} V_{\text{water}}}{K_{\text{H}}^{\text{TCE*}}} \right)_{\text{poly}} \right]}{\left(\frac{M_p}{\rho_p} \right) \left(\frac{C_{\text{TCE}}^{\text{Air}}}{K_{\text{H}}^{\text{TCE*}}} \right)_{\text{poly}}} \quad (1)$$

where $C_{\text{TCE}}^{\text{Air}}$ is the concentration of TCE in headspace (M), and $K_{\text{H}}^{\text{TCE*}}$ is Henry's law constants of TCE/water which is corrected for ionic strength (25) arising from the background electrolyte and polyelectrolyte. V_{hs} and V_{water} are the volume (L) of headspace and the volume of water (L) in the reactor, respectively. M_p is mass (g) of polymer in the reactor, and ρ_p is the density (g/L) of the polymer. The subscripts *ref* and *poly* refer to the reactors without and with polymer, respectively. The average K_p for each polyelectrolyte is obtained by averaging the K_p values from the reactors of 5 and 10 g/L of the same polyelectrolyte. Two concentrations of polymer were used in this experiment to also evaluate the effect of polymer concentration on K_p , which was negligible.

TCE Dechlorination. The TCE dechlorination rate and products were measured in 70 mL serum bottles containing 40 mL of headspace, 30 mL of liquid, and a Mininert closure. All reactors were prepared in an anaerobic glovebox (Argon-filled) and contained 2.8 g/L of either the bare RNIP, or polyelectrolyte-modified RNIP with an adsorbed polyelectrolyte surface excess concentration ranging from ~ 0.05 to ~ 2 mg/m^2 . It is important to note that degradation experiments were conducted using washed particles, i.e., no excess free polymer was in solution. Thus, the only polymer in the reactor was that adsorbed to the particles and did not affect TCE solubility in the bulk water. An aliquot of 0.15 mL of saturated TCE solution (8.4 mM) was added to provide the initial TCE concentration of 40 μM . Experiments were performed in duplicate. The reactors were rotated on an end-over-end rotator at 30 rpm at 23 ± 2 $^\circ\text{C}$. In control experiments without RNIP, it was demonstrated that TCE loss by mechanisms other than degradation by Fe^0 was negligible (e.g., photodegradation, adsorption, leakage). Mass transfer resistance at the vapor/liquid interface was not considered as these phases are assumed to be in equilibrium. A 100 μL headspace sample was withdrawn from the reactors and analyzed for TCE and its products using a 30 m GSQ PLOT capillary column on a HP 6890 GC/FID. Figure S1 (Supporting Information) provides example of TCE loss obtained from headspace measurements. A model previously reported for TCE degradation pathway by RNIP (10) (Figure S2a) was used to interpret the dechlorination kinetics in this study. It is assumed that all TCE reduction was via β -elimination to form acetylene and that both ethane and ethene resulted from reduction of acetylene. The reaction rate constants, k_{TCE} (TCE dechlorination to acetylene), k_2 (ethene formation from acetylene), and k_3 (ethane formation from acetylene) were determined using a kinetic modeling software package, Scientist, v.2.01 (Micromath, St. Louis, MO), by which the loss of TCE and formation of products (acetylene, ethene,

and ethane) were fit concurrently to determine the rate constants and 95% confidence intervals for the fits. The observed reaction rate constants determined from headspace measurements, $k_{\text{obs-h}}$, were converted to the observed rate constants without headspace, k_{obs} , for comparison between TCE and acetylene which have different Henry's law constants (Figure S2b) (16). The average rate constant and standard deviation (SD) were calculated from the upper and lower limits of the 95% confidence intervals (two values for each reactor) for rate constants measured in duplicate reactors. It should be noted that for RNIP the TCE dechlorination rate is independent of its Fe^0 content for Fe^0 contents greater than ~ 5 wt% (16). Therefore, small differences in the initial Fe^0 content of the particles, or loss of Fe^0 due to oxidation by water and TCE over the time scale of this study, do not affect RNIP's reactivity or the calculated rate constants.

Results and Discussion

Water/Polyelectrolyte Partitioning of TCE. The measured K_p for TCE partitioning to each polyelectrolyte is provided in Table 1. For the same type of polyelectrolyte, K_p increases with increasing molecular weight and hence degree of polymerization, D_p , however the increase in K_p was small and much less than the corresponding increase in D_p (Figure S3).

Effect of Adsorbed Polyelectrolytes on TCE Dechlorination. Carbon mass balance for all TCE degradation experiments was $\geq 90\%$. The observed TCE degradation rate constant for a representative polyelectrolyte coated RNIP (PSS70K-RNIP) normalized to that for bare RNIP is shown in Figure 2a. For all polyelectrolyte-modified RNIP, the dechlorination rate constant decreased nonlinearly with increasing surface excess concentration (Figure 2a and Figure S4). The curves generally have two distinct regions, an initial rapid decrease in reactivity at very low adsorbed polyelectrolyte mass, followed by a greater effect at high adsorbed mass of polyelectrolyte. This behavior has also been reported for the effect of natural organic matter on the reactivity of iron fillings (20) as well as the effect of physisorbed novel triblock copolymers on NZVI (9), and is consistent with Scheutjens and Fleer's conceptual model of homopolymer adsorption where polyelectrolyte adsorbs in a flat conformation (mostly trains) at low adsorbed mass to block reactive sites (region I), while at higher adsorbed masses the layer conformation becomes more extended (increasing fraction of loops and tails) whereby the polyelectrolyte layer may hinder TCE diffusion to the reactive surface or decrease the aqueous TCE concentration at the particle surface (region II). These processes are described in more detail next. For all of the polyelectrolytes evaluated, the maximum effect of adsorbed polyelectrolyte on the TCE degradation rate was a 24-fold decrease (filled symbols in Figure 2a and Figure S4). It is important to note that the adsorbed layer conformation will be a function of pH, which is 9.5–10.5 in this study. It is also noteworthy that the lower TCE dechlorination rate constant due to adsorbed polyelectrolytes observed here contrasts the increased TCE dechlorination rate constant observed for CMC-stabilized Fe–Pd bimetallic nanoparticles recently reported (26). This difference is probably because the Fe–Pd bimetallic nanoparticles were synthesized in the presence of CMC, yielding smaller particles that were stable against aggregation and thus more reactive than the larger nonstabilized Fe–Pd particles (26). The particles compared in this study were the same size but one had CMC physisorbed to the particle surface which decreased their reactivity.

Region I: Site Blocking by Trains. In region I, $k_{\text{TCE-obs}}$ decreases rapidly at very low surface excess concentration and generally plateaus with respect to the surface excess. This initial and rapid decrease of $k_{\text{TCE-obs}}$ is attributed to blocking of TCE reactive sites by adsorption of polyelectrolyte

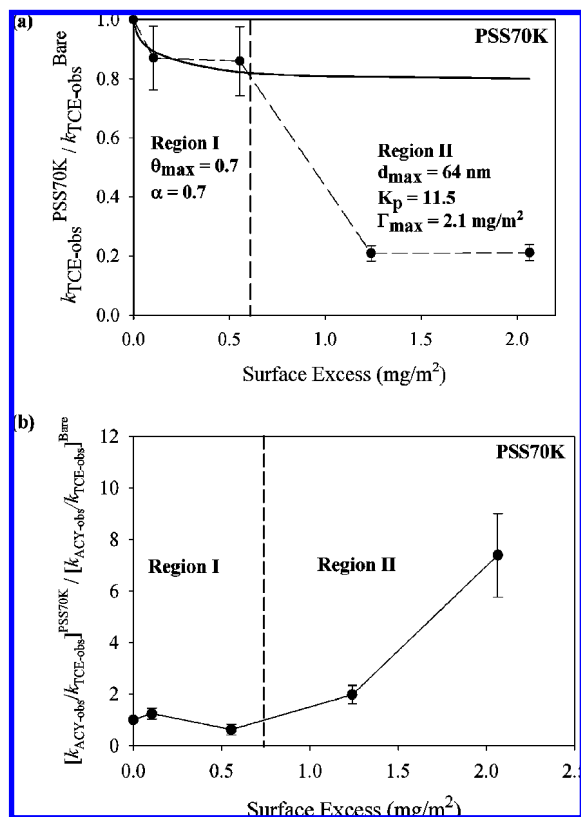


FIGURE 2. (a) Effect of adsorbed PSS70K on the observed TCE degradation rate constant as a function of polyelectrolyte surface excess concentration (filled symbols). Rate constants for PSS70K-modified RNIP are normalized to that measured for bare RNIP. Simulated normalized k_{TCE} due to site blocking (solid lines). (b) Acetylene transformation ($k_2 + k_3 = k_{ACY-obs}$) relative to its formation ($k_{TCE-obs}$) as a function of surface excess of polyelectrolytes for PSS70K-modified RNIP. Data are normalized to that observed for bare RNIP.

(as trains) on the RNIP surface. According to the Scheutjens–Fleer theory for homopolymer adsorption the degree of the surface covered by trains (θ) depends on the surface excess concentration (Γ) for a given polyelectrolyte type and fixed ionic strength and temperature (21). The relationship between the surface coverage and the surface excess is eq 2.

$$\theta = \frac{\theta_{max}\Gamma}{\theta_{slope} + \Gamma} \quad (2)$$

where θ_{max} is the maximum surface coverage (as trains) and θ_{slope} is a fitting parameter. The surface coverage by trains typically develops rapidly (controlled by the value of θ_{slope}) and ultimately reaches a plateau of θ_{max} at high surface excess. Complete surface coverage will not occur so the apparent dechlorination rate constant of surface-modified RNIP ($k_{TCE-surf}^{polyelectro}$) includes contributions from bare unbound sites ($1 - \theta$) where the TCE degradation rate constant equals that for the bare RNIP ($k_{TCE-surf}^{bare}$), and bound sites (θ) that are in direct contact with trains where the electron transfer efficiency and the reaction rate constant at the bound sites is less than that for bare surfaces ($k_{TCE-surf}^{bound} < k_{TCE-surf}^{bare}$). If we define an electron transfer efficiency, $\alpha = k_{TCE-surf}^{bound} / k_{TCE-surf}^{bare}$, the apparent dechlorination rate constant of surface modified RNIP ($k_{TCE-surf}^{polyelectro}$) is given by eq 3.

$$k_{TCE-surf}^{polyelectro} = [(1 - \theta) + (\alpha\theta)]k_{TCE-surf}^{bare} \quad (3)$$

The magnitude of the constant α is controlled by the separation between the TCE molecule and the underlying

RNIP surface (23) and therefore is likely specific to the polyelectrolyte type.

Assuming that site blocking is the only phenomenon affecting the TCE dechlorination rate at low adsorbed mass (region I), $k_{TCE-obs}$ as a function of surface excess in region I can be fit by least-squares considering the development of trains as a function of the measured surface excess (eq 2) and corresponding blocking (eq 3). Region I is defined by the fitting procedure whereby the least-squares fit of region I (solid lines in Figure 2 and Figure S4) included data points from zero adsorbed mass and higher until inclusion of data at higher adsorbed mass decreased the goodness of fit. The data points which were not incorporated into region I were assigned as region II. There are distinct regions (I and II) for each type of polyelectrolyte-modified RNIP (Figure 2a and Figure S4). The fitting parameters include θ_{max} , θ_{slope} , and α . While these individual parameters cannot be determined individually with confidence, the resulting parameters are consistent with expectations as described next.

Train development as a function of surface excess corresponding to these fits is shown in Figure S5a. The value of θ_{max} obtained from the least-squares fit is ~ 0.7 for the medium and large polyelectrolytes (PSS and CMC) and from 0.8 to 0.9 for small polyelectrolytes (PAP). These are in the range predicted by the Scheutjens–Fleer theory for medium and large polymers (0.7–0.8 for adsorption to a nonspecific adsorbent) and for small polymers (0.9–1 for sorption to a nonspecific adsorbent), respectively (21). It should be noted that for medium and large polyelectrolytes comprised of the same monomer, e.g., PSS70K and PSS1 M as well as CMC90K and CMC700K, θ_{max} (~ 0.7 for both PSS and CMC) was independent of the degree of polymerization. Theoretically (21), θ_{max} is controlled by degree of polymerization (D_p), the Flory–Huggins polymer–solvent interaction parameter (χ), and the effective adsorption energy parameter (χ_s^{eff}) which includes the electrostatic interaction due to surface charge of an adsorbent, charge of the polyelectrolyte, and the influence of ionic strength (21). However, for polymers with $D_p > 100$ units θ_{max} becomes less sensitive to D_p (21) and θ_{max} is mainly governed by χ and χ_s^{eff} . The χ and χ_s^{eff} are similar for polymers with the same monomer units, thus leading to similar values of θ_{max} for PSS70K and PSS1 M and for CMC90K and CMC700K.

Region II: Site Blocking by Trains Coupled with Mass Transfer Resistance and TCE Adsorption by Loops and Tails.

A second decrease in reactivity is observed at high surface excess of adsorbed polyelectrolyte (Figure 2a and Figure S4) that cannot be explained by site blocking alone (solid lines) since surface coverage by trains does not increase at high surface excess (Figure S5a). However, the number of loops and tails increases as a polymer layer of some finite thickness (d) develops around the particle (Figure 1b) (21). TCE partitions preferentially to the adsorbed polyelectrolyte layer (K_p in Table 1), and might therefore be expected to produce an increase in reactivity due to the increased concentration of TCE at the particle surface. This is not observed. Rather, further decrease in reactivity ($k_{TCE-obs}$) is observed at high surface excess in region II and either attributed to inhibition of TCE diffusion through the more extended, stagnant layer to the particle surface or to a decrease in aqueous TCE at the particle surface due to TCE partitioning to the adsorbed polyelectrolyte. Conceptually this is analogous to mass transfer through a thin film coupled with surface reaction. However, the distribution of adsorbed polyelectrolyte is not homogeneous throughout the layer thickness. Rather, the volume fraction of adsorbed homopolymers decreases exponentially as a function of distance from the surface (21). The layer consists of two regions: the inner (concentrated) near-surface region (< 2.5 nm) where loops dominate and the outer (dilute) region where only tails contribute to the

profile of adsorbed layer (21). The rate of TCE diffusion through the adsorbed polyelectrolyte layers should be fast relative to the reaction rates observed (hours) given the short transport distance (<2.5 nm). Therefore, diffusion of TCE through the layer is not likely to limit TCE dechlorination. Thus the effect of adsorbed loops and trains on the TCE dechlorination rate is most likely due to a decrease of available dissolved TCE at the particle surface for reaction. Adapted from a solution of mass transfer through a thin film coupled with surface reaction and assuming that diffusion resistance is negligible (see derivation in Supporting Information), the relationship between $k_{TCE-obs}^{polyelectro}$, $k_{TCE-surf}^{polyelectro}$, and mass transfer characteristics of the adsorbed polymer layer is eq 4:

$$k_{TCE-obs}^{polyelectro} \approx k_{TCE-surf}^{polyelectro} H_{surf} \quad (4)$$

where H_{surf} (dimensionless and <1) is the partition coefficient between dissolved TCE in water inside the concentrated layer ($C_{water-layer}$) and dissolved TCE in bulk water outside the layer (C_{bulk}) assuming local equilibrium for partitioning of TCE between water and the polyelectrolyte.

$$\frac{1}{H_{surf}} = 1 + K_p r_{pw}^{surf} \quad (5)$$

r_{pw}^{surf} is the average polyelectrolyte-to-water ratio (V/V) in the thin near-surface layer (ΔL) from the RNIP surface where the adsorbed polymer density is sufficient to control the availability of TCE from the bulk solution to the particle surface. r_{pw}^{surf} is calculated from r_{pw} (the average, polyelectrolyte-to-water ratio (V/V) in the adsorbed polyelectrolyte layer) which is a function of distance from the RNIP surface because the volume fraction of adsorbed homopolymer $\Phi(x)$ decreases exponentially as a function of distance from the surface (21),

$$\Phi(x) = \frac{A \frac{\Gamma}{\rho_p} \exp(-Ax)}{\frac{4}{3} \pi [(x + \Delta x + a_p)^3 - (x + a_p)^3]} \quad (6)$$

$$\int_0^d \Phi(x) dx = \frac{\frac{\Gamma}{\rho_p}}{\frac{4}{3} \pi [(d + a_p)^3 - (a_p)^3]} \quad (7)$$

$$r_{pw} = \frac{\Phi(x)}{1 - \Phi(x)} \quad (8)$$

where Γ is surface excess of adsorbed polyelectrolyte on the surface of RNIP, a_p is the average radius of RNIP, and ρ_p is the density of polyelectrolytes. The constant A is obtained by iteration of eqs 6 and 7. Here, all the parameters with subscript *surf* are calculated at $x = \Delta L = 2.5$ nm. Due to the exponential distribution of adsorbed polyelectrolyte from the surface of RNIP (Figure S6b and Figure S7), the aqueous TCE concentration inside the adsorbed polyelectrolyte layer is lowest (lowest H simulated in Figure S7) at the surface of RNIP as this is the region with the highest r_{pw}^{surf} . Consequently, the apparent dechlorination rate is controlled by the availability, of TCE in the thin but dense polyelectrolyte layer ΔL on the particle surface. The choice of $\Delta L = 2.5$ nm yields the best modeling fits for all polyelectrolyte-modified RNIP at the highest surface excess (the last data points of Figure 2a and Figure S4) using eq 4 (Figure 3). The choice of $\Delta L = 2.5$ nm is reasonable in that it is greater than the backbone on the polyelectrolytes which is $\sim 2-3$ Å if both carbon backbones and side chains (e.g., the sulfonate group of PSS or carboxylic group of CMC and PAP) are adsorbed flat on the RNIP surface, and as high as ~ 1 nm if the carbon backbones are adsorbed flat but the side chains extend

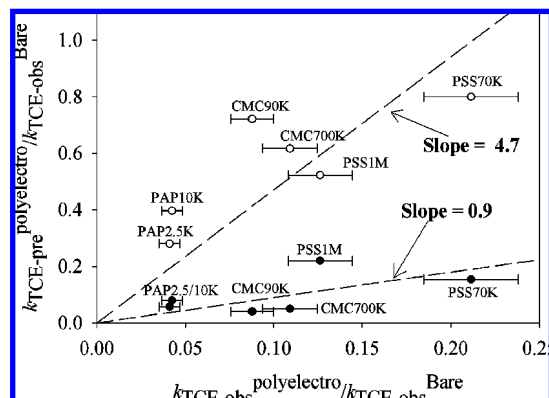


FIGURE 3. Relationship between $k_{TCE-obs}^{polyelectro}$ at the maximum surface excess and the simulated $k_{TCE-pre}^{polyelectro}$ assuming site blocking only (open symbols) and site blocking and decreased TCE concentration at the particle surface due to partitioning to adsorbed loops and trains (filled symbols). Site-blocking alone overpredicts the rate constants at higher surface excess.

perpendicular to the RNIP surface due to electrostatic repulsion between the negatively charged surface and the negatively charged functional groups of the side chains. And it is in the range expected for, for inner layer dominated by loops (Figure S7a) where the adsorbed layer is densest and can decrease the availability of aqueous TCE due to partitioning. It should be noted that the choice of ΔL from 0.5 to 2.5 nm does not significantly affect the value of this approximation. Using a $\Delta L > 5$ nm affects the value of the approximation, but does not alter the qualitative conclusions.

The correlation between the observed TCE degradation rate constant, $k_{TCE-obs}^{polyelectro}$, for particles having the maximum adsorbed mass of polyelectrolyte versus the predicted $k_{TCE-pre}^{polyelectro}$ (eq 4) using H_{surf} calculated from the measured surface excess (Γ), K_p , the estimated layer thickness (d) from ref (2) at the maximum surface excess (Figure 3-filled symbols), and $k_{TCE-pre}^{polyelectro}$ assuming only site blocking due to trains (eq 3) (Figure 3-open symbols) is illustrated in Figure 3. The corresponding Φ , r_{pw} , and H as a function of distance from surface are also illustrated in Figure S7. Assuming site-blocking alone (Figure 3-open symbols) significantly overpredicts rate constants (slope of 4.7) because it does not consider the effect of partition of TCE to the adsorbed loops and trains of the polyelectrolyte brush at the particle surface. The predicted and observed reaction rates are reasonable when both site blocking and decreased TCE availability are considered (slope of 0.9). This suggests that a conceptual model of site blocking and decreased TCE availability captures the dominant physical phenomena responsible for the decreased reactivity of polyelectrolyte-modified RNIP at the maximum surface excess.

Effect of Adsorbed Polyelectrolytes on Byproduct Distribution. As with bare RNIP tested under similar iron loadings (17), TCE dechlorination by all polyelectrolyte-modified RNIP produced no chlorinated reaction intermediates, acetylene as the primary TCE dechlorination intermediate, and ethane and ethene as the major dechlorination products. Thus, the dechlorination pathways are not affected by the presence of the adsorbed polyelectrolyte and β -elimination remains the dominant TCE dechlorination pathway (16, 17). Adsorbed polyelectrolyte did, however alter acetylene accumulation, i.e., the ratio of the acetylene transformation rate constant ($k_2 + k_3 = k_{ACY-obs}$) to the acetylene formation rate constant ($k_{TCE-obs}$). The magnitude of this effect depended on the surface excess (Figure 2b). Figure 2b shows this effect for PSS70K-modified RNIP, but the trend is the same for all of the polyelectrolytes evaluated (Figure S8). There are two distinct regions in these figures that qualitatively support the conclusion that surface reac-

tivity is affected by both site blocking by trains (region I) and limited TCE availability due to adsorbed polyelectrolyte (region II). In region I (low surface excess of adsorbed polyelectrolyte and the absence of an extended layer), the ratio of acetylene transformation to its formation for modified particles relative to bare particles is close to unity. In this region, adsorbed polyelectrolyte trains affect surface reaction only by blocking reactive sites, and both acetylene formation and transformation are affected equally. In contrast, in region II (high surface excess of adsorbed polyelectrolyte where an extended polyelectrolyte layer forms), the ratio of acetylene transformation to its formation for modified particles relative to bare particles becomes significantly greater than unity. In this region, the polyelectrolyte layer limits the availability of aqueous TCE at the RNIP surface. Because TCE ($k_{ow} = 263$ (25)) is much more hydrophobic than acetylene ($k_{ow} = 2.34$ (25)), the TCE availability is affected by partitioning to the adsorbed polyelectrolyte layer much more so than acetylene so the rate of TCE dechlorination (hence acetylene formation) is decreased more than for acetylene transformation, resulting in less acetylene accumulation and greater ethene and ethane formation per mol of TCE degraded compared to bare RNIP.

Implications for Applications of NZVI. The magnitude of the effect of reactive site blocking and decreased TCE availability on the TCE dechlorination rate constant depends on the characteristics of the adsorbed polyelectrolyte layer, which depend on the adsorbed mass, adsorbed layer thickness, and the type of monomer in the polyelectrolyte (2). In practice, polyelectrolyte-modified RNIP will likely be applied at the maximum adsorbed surface excess to enhance the colloidal stability and transport in the subsurface. At the maximum adsorbed mass, $k_{TCE-obs}$ for each of the polyelectrolyte-modified RNIP was 5–24 times less than for bare RNIP (Table 2). The half-life values (τ) for TCE for each type of polyelectrolyte-modified RNIP (2 g/L) are also calculated and summarized in Table 2. Despite the decrease in activity due to surface modification by polyelectrolytes, the TCE dechlorination rate and TCE half-life times at the typical application rate (2 g/L in porewater) should be sufficient for in situ application. Therefore, for the group of modifiers evaluated here, the effect of the modifier on TCE reactivity is not likely to influence the choice of modifier because they are not substantially different from one another. Rather, the governing criteria might be the ability of the modifier to enhance transport (8) and potentially to increase the contact between NZVI and TCE (3). It should be noted that the conformation of the adsorbed polyelectrolyte will affect the polymer density at the surface and therefore their effect on reactivity. The conformation can be affected by groundwater constituents such as Ca^{2+} and Mg^{2+} , and from Fe^{2+} . For example, Ca^{2+} and Mg^{2+} in groundwater can screen the charge of ionized groups in the polyelectrolyte (21) or promote dehydration of both the ions and the polyelectrolyte chains (27). This would cause the adsorbed polyelectrolyte layer to collapse onto the particle surface, thereby increasing polymer density at the NZVI surface. This is especially true for weak polyelectrolytes such as PAP and CMC. While the effect of Fe^{2+} from Fe^0 oxidation is accounted for in this study, the effect of Ca^{2+} or Mg^{2+} is not and should be evaluated.

Regarding environmental implications of nanotechnology, surface modification decreases NZVI reactivity. This could explain the decreased toxicity (assessed by oxidative stress end points for microglia and neurons) of surface-modified NZVI compared to bare NZVI as recently reported (28). This suggests that although surface modification enhances NZVI migration which might increase the likelihood of NZVI exposure to organisms, it might decrease the intrinsic toxicity of the particles. However, whether surface modification will increase or decrease overall risk of NZVI depends on the magnitude of its effects on both exposure and toxicity.

Acknowledgments

This research was funded in part by the U.S. EPA (R830898 and R833326, the NSF (BES-068646 and EF-0830093), the Department of Defense through the Strategic Environmental Research and Development Program (W912HQ-06-C-0038), and the Royal Thai Government through a fellowship to T.P.

Supporting Information Available

Simplified TCE reduction pathways, the linear trend between K_p and D_p , the simulation of train and layer thickness development, the simulation of volume fraction profile of adsorbed polyelectrolytes, and the derivation of eq 4. This material is available free of charge via the Internet at <http://pubs.acs.org>.

Literature Cited

- Wiesner, M. R.; Lowry, G. V.; Alvarez, P.; Dionysiou, D.; Biswas, P. Assessing the risks of manufactured nanomaterials. *Environ. Sci. Technol.* **2006**, *40* (14), 4336–4345.
- Phenrat, T.; Saleh, N.; Sirk, K.; Kim, H.-J.; Tilton, R. D.; Lowry, G. V. Stabilization of aqueous nanoscale zerovalent iron dispersions by anionic polyelectrolytes: adsorbed anionic polyelectrolyte layer properties and their effect on aggregation and sedimentation. *J. Nanopart. Res.* **2008**, *10*, 795–814.
- Saleh, N.; Phenrat, T.; Sirk, K.; Dufour, B.; Matyjaszewski, K.; Tilton, R. D.; Lowry, G. V. Adsorbed triblock copolymers deliver reactive iron nanoparticles to the oil/water interface. *Nano Lett.* **2005**, *12*, 2489–2494.
- He, F.; Zhao, D.; Liu, J.; Roberts, C. B. Stabilization of Fe-Pd Nanoparticles with Sodium Carboxymethyl Cellulose for Enhanced Transport and Dechlorination of Trichloroethylene in Soil and Groundwater. *Ind. Eng. Chem. Res.* **2007**, *46* (1), 29–34.
- Hydutsky, B. W.; Mack, E. J.; Beckerman, B. B.; Skluzacek, J. M.; Mallouk, T. E. Optimization of Nano- and Microiron Transport through Sand Columns Using Polyelectrolyte Mixtures. *Environ. Sci. Technol.* **2007**, *41* (18), 6418–6424.
- Hyung, H.; Fortner, J. D.; Hughes, J. B.; Kim, J. H. Natural Organic Matter Stabilizes Carbon Nanotubes in the Aqueous Phase. *Environ. Sci. Technol.* **2007**, *41*, 179–184.
- Levenspiel, O., *Chemical Reaction Engineering*, 3rd ed.; Wiley: New York, 1998.
- Saleh, N.; Kim, H.-J.; Phenrat, T.; Matyjaszewski, K.; Tilton, R. D.; Lowry, G. V. Ionic Strength and Composition Affect the Mobility of Surface-Modified Fe⁰ Nanoparticles in Water-Saturated Sand Columns. *Environ. Sci. Technol.* **2008**, *42* (9), 3349–3355.
- Saleh, N.; Sirk, K.; Liu, Y.; Phenrat, T.; Dufour, B.; Matyjaszewski, K.; Tilton, R. D.; Lowry, G. V. Surface modifications enhance nanoiron transport and NAPL targeting in saturated porous media. *Environ. Eng. Sci.* **2007**, *24* (1), 45–57.
- Liu, Y.; Phenrat, T.; Lowry, G. V. Effect of TCE concentration and dissolved groundwater solutes on NZVI-promoted TCE dechlorination and H₂ evolution. *Environ. Sci. Technol.* **2007**, *41* (22), 7881–7887.
- Nurmi, J. T.; Tratnyek, P. G.; Sarathy, V.; Baer, D. R.; Amonette, J. E.; Pecher, K.; Wang, C.; Linehan, J. C.; Matson, D. W.; Penn, R. L.; Driessen, M. D. Characterization and properties of metallic iron nanoparticles: spectroscopy, electrochemistry, and kinetics. *Environ. Sci. Technol.* **2005**, *39* (5), 1221–1230.
- Lowry, G. V.; Johnson, K. M. Congener-Specific Dechlorination of Dissolved PCBs by Microscale and Nanoscale Zerovalent Iron in a Water/Methanol Solution. *Environ. Sci. Technol.* **2004**, *38* (19), 5208–5216.
- Song, H.; Carraway, E. R. Catalytic hydrodechlorination of chlorinated ethenes by nanoscale zero-valent iron. *Appl. Catal. B* **2008**, *78* (1–2), 53–60.
- Li, X.-q.; Zhang, W.-x. Sequestration of Metal Cations with Zerovalent Iron Nanoparticles—A Study with High Resolution X-ray Photoelectron Spectroscopy (HR-XPS). *J. Phys. Chem. C* **2007**, *111* (19), 6939–6946.
- Joo, S. H.; Zhao, D. Destruction of lindane and atrazine using stabilized iron nanoparticles under aerobic and anaerobic conditions: Effects of catalyst and stabilizer. *Chemosphere* **2008**, *70*, 418–425.
- Liu, Y.; Lowry, G. V. Effect of particle age (Fe⁰ content) and solution pH on NZVI reactivity: H₂ evolution and TCE dechlorination. *Environ. Sci. Technol.* **2006**, *40* (19), 6085–6090.

- (17) Liu, Y.; Majetich, S. A.; Tilton, R. D.; Sholl, D. S.; Lowry, G. V. TCE dechlorination rates, pathways, and efficiency of nanoscale iron particles with different properties. *Environ. Sci. Technol.* **2005**, *39*, 1338–1345.
- (18) Arnold, W. A.; Roberts, A. L. Pathway and kinetics of chlorinated ethylene and chlorinated acetylene reaction with Fe(0) particles. *Environ. Sci. Technol.* **2000**, *34*, 1794–1805.
- (19) Xu, J.; Dozier, A.; Bhattacharyya, D. Synthesis of Nanoscale Bimetallic Particles in Polyelectrolyte Membrane Matrix for Reductive Transformation of Halogenated Organic Compounds. *J. Nanopart. Res* **2005**, *7* (4–5), 449–467.
- (20) Tratnyek, P. G.; Scherer, M. M.; Deng, B.; Hu, S. Effects of Natural Organic Matter, Anthropogenic Surfactants, and Model Quinones on the Reduction of Contaminants by Zero-Valent Iron. *Water Res.* **2001**, *35* (18), 4435–4443.
- (21) Fleer, G. J.; Cohen Stuart, M. A.; Scheutjens, J. M. H. M.; Cosgrove, T.; Vincent, B. *Polymers at Interfaces*; Chapman & Hall: New York, 1998.
- (22) Ohshima, H. Electrophoresis of soft particles. *Adv. Colloid Interface Sci.* **1995**, *62*, 189–235.
- (23) Rusling, J. F. Molecular aspects of electron transfer at electrodes in micellar solutions. *Colloids Surf.* **1997**, *123–124*, 81–88.
- (24) Phenrat, T.; Saleh, N.; Sirk, K.; Tilton, R., D.; Lowry, G., V. Aggregation and sedimentation of aqueous nanoscale zerovalent iron dispersions. *Environ. Sci. Technol.* **2007**, *41* (1), 284–290.
- (25) Schwarzenbach, R. P.; Gschwend, P. M.; Imboden, D. M. *Environmental Organic Chemistry*, 2nd ed.; Wiley-Interscience: Hoboken, NJ, 2003.
- (26) He, F.; Zhao, D. Hydrodechlorination of trichloroethene using stabilized Fe-Pd nanoparticles: Reaction mechanism and effects of stabilizers, catalysts, and reaction conditions. *Appl. Catal. B* **2008**, *84* (3–4), 533–540.
- (27) Konradi, R.; Rühle, J. Interaction of Poly(methacrylic acid) Brushes with Metal Ions: Swelling Properties. *Macromolecules* **2005**, *38* (10), 4345–4354.
- (28) Phenrat, T.; Long, T. C.; Lowry, G. V.; Veronesi, B. Partial oxidation (“aging”) and surface modification decrease the toxicity of nanosized zerovalent iron. *Environ. Sci. Technol.* **2009**, *43* (1), 195–200.

ES802187D